Tectonophysics 672–673 (2016) 16–23

Contents lists available at ScienceDirect

Tectonophysics

journal homepage: www.elsevier.com/locate/tecto

Magmatic underplating beneath the Emeishan large igneous province (South China) revealed by the COMGRA-ELIP experiment

Yangfan Deng [a,*], Yun Chen [b], Peng Wang [c], Khalid S. Essa [d], Tao Xu [b], Xiaofeng Liang [b], José Badal [e]

[a] State Key Laboratory of Isotope Geochemistry, Guangzhou Institute of Geochemistry, Chinese Academy of Sciences, Guangzhou 510640, China
[b] State Key Laboratory of Lithospheric Evolution, Institute of Geology and Geophysics, Chinese Academy of Sciences, Beijing 100029, China
[c] Institute of Earthquake Science, China Earthquake Administration, Beijing 100036, China
[d] Department of Geophysics, Faculty of Science, Cairo University, Giza, Egypt
[e] Physics of the Earth, University of Zaragoza, Pedro Cerbuna 12, 50009 Zaragoza, Spain

ARTICLE INFO

Article history:
Received 17 July 2015
Received in revised form 18 January 2016
Accepted 28 January 2016
Available online 4 February 2016

Keywords:
Stripping
Residual gravity
Density anomaly
Underplating
Emeishan large igneous province
South China

ABSTRACT

Because of the abundant geological, geochemical and geophysical studies conducted on the Emeishan large igneous province (ELIP) in South China, the Permian mantle plume model associated with this region is widely accepted. Furthermore, the dome-shaped structure related with this plume has been determined with success by sedimentological data and gravity stripping. Although the sediment thickness, upper crust, Moho depth and the lithosphere–asthenosphere boundary (LAB) are well constrained by active- and passive-source seismological results, the density anomaly in ELIP is still a poorly constrained issue that needs further attention. With the aim especially to understand the impact on surface of the magmatic processes that originated in the deep mantle, we performed the COMGRA-ELIP gravity experiment across this region. Using a stripping method, we determined the residual gravity in ELIP and surrounding areas. The residual gravity reaches a maximum value of +150 mGal in the inner zone of ELIP and its strength decreases gradually when measuring from the inner zone to the middle and outer zones. Combining active and passive seismic results and the least-squares variance analysis method, we propose a strong density contrast of 0.2 g/cm^3 (density of 3.14 g/cm^3) for the 15- to 20-km-thick igneous layer accreted at the base of the crust, as evidence of crustal underplating in ELIP, to explain the present-day residual gravity anomaly.

1. Introduction

The Emeishan large igneous province (hereafter ELIP) lies within a rhombus-shaped area of 250,000 km^2 bounded by the Lijiang–Xiaojinhe fault to the northwest and the Red River fault to the southwest (Xu et al., 2001) (Fig. 1). In recent years, ELIP has drawn the attention of the scientific community because of its great importance in understanding the origin of intraplate igneous structures and its possible synchrony with the end-Permian mass extinctions (Wignall et al., 2009; Wu and Zhang, 2012; Cheng et al., 2014; Shellnutt et al., 2012; Shellnutt, 2014; Xu et al., 2014a; Yuan et al., 2014; Zhong et al., 2014). According to the extent of erosion of the Maokou Formation composed of Mid–Late Permian carbonates (He et al., 2003, 2006; Xu et al., 2004), the dome-shaped structure associated with ELIP can be divided into three zones, namely, the inner, middle and outer zones, and the Xiaojiang fault is the boundary between the inner and middle zones (Fig. 1). The extent of the erosion is more apparent in the inner zone, which is proposed as the site of a rising plume head (He et al., 2003).

It has been suggested that igneous intrusion at the base of the crust may underlie the flood basalts (White and McKenzie, 1989; Coffin and Eldholm, 1994). Magmatic underplating occurs when basaltic magmas are trapped at the Mohorovičić discontinuity or within the crust during its rise to the surface (Cox, 1993). Underplating of magma is an important process for crustal formation and subsequent evolution because the inflow of magma provides a non-tectonic way for growing and thickening of the crust (Thybo and Artemieva, 2013). Geophysical studies (as well as igneous petrology and geochemistry) utilize the differences in density and seismic velocity to identify underplating that occurs at depth (Behera et al., 2004; Singh et al., 2004; Thybo and Artemieva, 2013), but the density studying in ELIP is still poor.

In an attempt to characterize the subsurface structure that is related to fossil mantle plume activity, a comprehensive geophysical investigation was conducted in ELIP, and the properties and geometry of the crust collectively suggest the existence of a 15- to 20-km-thick and a 150- to 180-km-wide mafic layer overlying the base of the crust in the inner zone (Chen et al., 2015). In this paper, since the depth of interfaces and magmatic underplating process seem to be well constrained by comprehensive geophysical investigation (Xu et al., 2015; Chen et al., 2015; Chen et al., in preparation), we assess the density of the mafic

* Corresponding author at: 511 Kehua Street, Tianhe District, Guangzhou, China.
E-mail address: yangfandeng@gig.ac.cn (Y. Deng).

http://dx.doi.org/10.1016/j.tecto.2016.01.039
0040-1951/

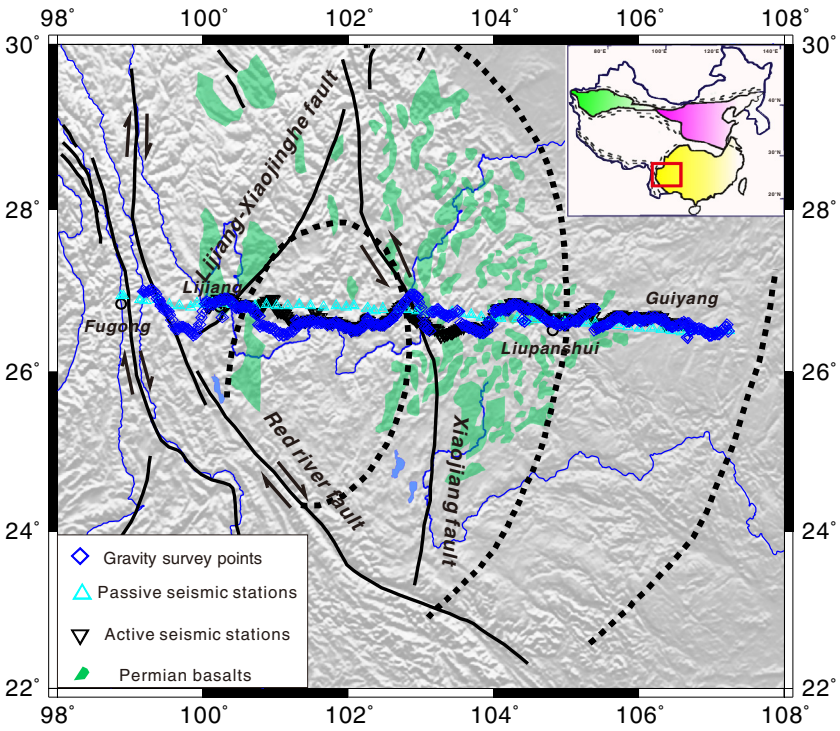

Fig. 1. Tectonic features (main faults) depicted on a topographic map of the Emeishan large igneous province (ELIP). The inset in the top right corner shows a small rectangle on a map of China that reveals the location of the explored area. The dash lines indicate the inner, middle and outer zones of ELIP. Three instrument sets were deployed from west to east in this region: a gravity profile (blue diamonds indicate gravity survey points), a passive-source seismic array (pale blue triangles indicate passive seismic stations) and an active-source seismic array (black inverted triangles indicate active seismic stations). The distribution of Permian basalts is similar to that of Xu et al. (2004, 2007).

layer based on the observed gravity data from the COMGRA-ELIP experiment. Starting from the results obtained by seismology, by least-squares variance analysis and with the help of the trial-and-error method, we estimate both the density and the shape of underplating in the lower crust that fits the residual gravity.

2. Data processing and Bouguer gravity

In order to understand the gravity response to the magmatic process in ELIP, during the months of July and August 2012, we carried out the COMGRA-ELIP experiment for gravity measurement along a west–east 800-km-long profile that crosses the inner, middle and outer zones of ELIP (Fig. 1). This experiment included 338 measurement points measured by a Burris gravity meter (No. B65) whose accuracy reaches 15 μGal (Zhang et al., 2011). The observation points were spaced an average distance of about 2.2 km. Gravity readings were recorded relative to two base points belonging to the national gravity network of China, one located at the east part of the profile near Guiyang (Guizhou Province) and another at the west part near Lijiang (Yunnan Province). In order to carry out the terrain correction, in addition to measuring the relative gravity, we also recorded the elevation of each survey point using a Trimble GeoXM GPS with precision of up to 1 m.

After a series of gravity reductions that include drift correction, tide correction, latitude correction, topography correction and Bouguer correction (Zeng, 2005), the obtained Bouguer gravity is shown in Fig. 2. The elevations along the reference profile fluctuate greatly in the inner and middle zones; the sharpest variation occurs in the middle of the profile and correlates with the Xiaojiang fault, which can be seen clearly as the boundary between these two zones (Fig. 2, upper plot). The Bouguer gravity anomaly increases gradually from west to east, from −330 to −130 mGal, with a dome-shaped variation in the inner zone (Fig. 2, lower plot). To some extent, the respective shapes of the topography and the Bouguer gravity keep mirror symmetry.

The measured Bouguer gravity is a summation of all density anomalies within the lithosphere including the density difference of the layers with respect to those of the reference model and the undulation of intra-crustal and sub-crustal layers. Low-density sediments result in a negative gravity anomaly relative to the crystalline crust, and removing this effect due to the sediments will increase the residual anomaly. Contrarily, an uplift of the Moho produces a positive gravity anomaly and its elimination will lead to a reduction in the residual anomaly. In contrast, a depression of the Moho produces a negative anomaly (Mooney and Kaban, 2010). Although the topography and free-air effects have been removed from the Bouguer gravity, in order to isolate the gravity response of ELIP we have to remove particular gravitational effects caused by the sedimentary cover, the undulation of the upper crust, the Moho and the mantle lithosphere from shallower to deeper depths. This sequential procedure, named *stripping*, was first described by Hammer (1963) and later developed by other authors (Bielik, 1988; Mooney and Kaban, 2010; Bielik et al., 2013a, 2013b; Deng et al., 2014a).

3. Gravitational effects

It is generally assumed that any change affecting the horizontality of the homogeneous reference density model would lead to a change in the residual gravity anomaly (Mooney and Kaban, 2010), whereas the gravity from a uniform horizontal layer with invariable density is a constant. Our reference model corresponds to a continental crust with flat topography (Fig. 3), which consists of a 15-km-thick upper crust with density 2.7 g/cm^3 (Mooney and Kaban, 2010) above a 25-km-thick lower crust with density 2.94 g/cm^3 (Mooney and Kaban, 2010; Deng et al., 2011). The average density of the lithospheric mantle is set to

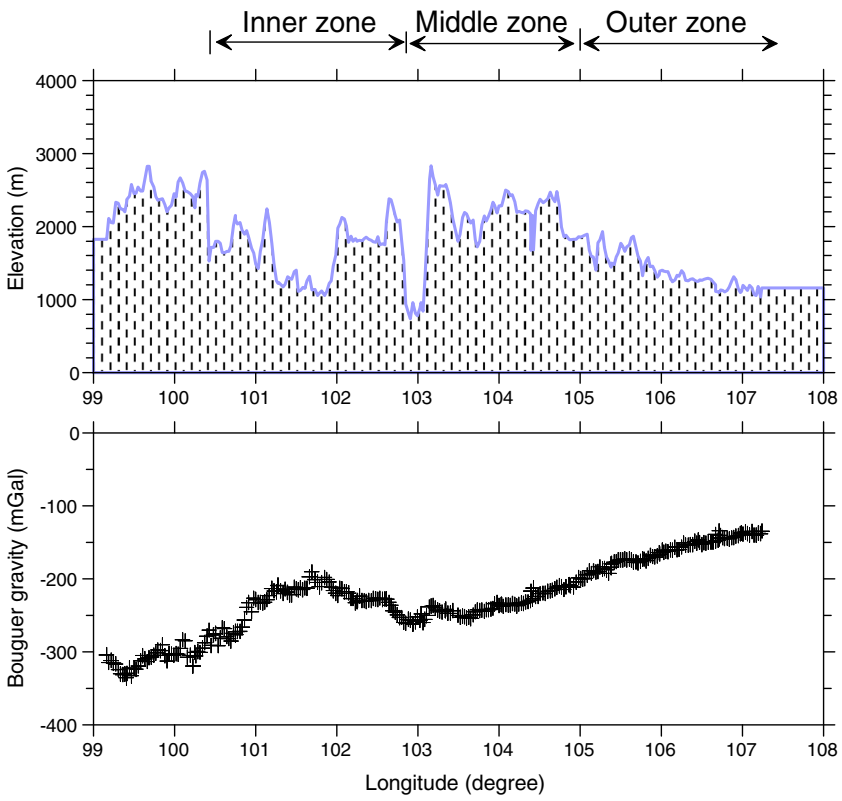

Fig. 2. Topography and Bouguer gravity anomaly along the gravity profile that crosses ELIP from west to east (Fig. 1).

3.33 g/cm^3, while that of the asthenosphere is 3.31 g/cm^3 (Burov, 2010, 2011).

3.1. Gravitational effect of the sediments

When processing the Bouguer gravity field, the first step is to remove the effect of the sedimentary cover by forward modeling its gravity anomaly, which is a linear problem (Nagy, 1966; Li and Oldenburg, 1998). There are several methods to calculate the gravity anomaly, such as the cuboid method (Deng et al., 2014a, 2014b) and the polygon method (Jia and Meng, 2009; Wang et al., 2014a, 2014b). In this study, we use the latter one, assuming that the gravity anomaly is generated by a horizontal polygonal prism lying parallel to the y axis, such that the subsurface mass can be divided into a finite number of these prisms (Jia and Meng, 2009). Operating in the x–z plane (z axis is downward), the gravity anomaly at the origin point (0, 0) is given by:

$$g(0,0) = 2G\rho\sum_{i=1}^{N} r_{i1}\left(\sin\theta_{i1}\cos\varphi_i - \cos\theta_{i1}\sin\varphi_i\right) \times \left(\sin\varphi_i \ln\frac{r_{i1}}{r_{i2}} + \Delta\theta_i\cos\varphi_i\right)$$

where G is the gravitational constant, ρ is the density in the 2D polygonal element within the x–z plane and the remaining parameters related with the geometry are clearly described in Jia and Meng (2009).

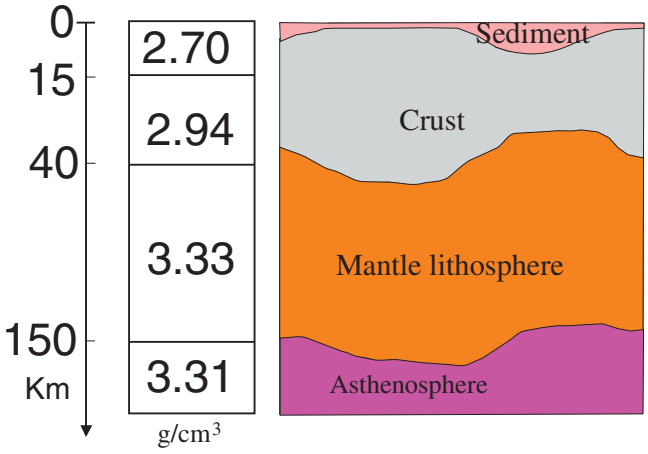

Fig. 3. Left: the reference lithospheric/asthenospheric structure described in terms of the respective depths and densities of the major layers. Right: sketch illustrating the laterally varying lithosphere.

Since the COMWIDE-ELIP experiment has provided a detailed velocity model for the upper crust (Xu et al., 2014b), in our calculation, we took the velocity contour 5.8 km/s as the lower limit of the sedimentary cover (Zhang and Klemperer, 2010; Zhang et al., 2013), together with a density of sediments equal to 2.4 g/cm^3. Nevertheless, the length spanned by the mentioned seismic experiment is not as long as that of our gravity profile, by which we took into account the sediment thickness provided by the Simao–Zhongdian profile (Zhang et al., 2006) for the western transect and the thickness supplied by the CRUST1.0 model for the eastern transect (Laske et al., 2013). Fig. 4a (lower plot) shows the contour of the sediment thickness across the Lijiang–Qingzhen profile, which varies considerably from one location to another. The average thickness is about 2 km, although the deepest depth could be 7 km. Using the linear forward method mentioned above, we calculated the gravitational effect of the sediments (Fig. 4a, upper plot). The density contrast is 0.3 g/cm^3 with respect to the reference model (Fig. 3). The maximum of the gravity anomaly is about −40 mGal in the inner and middle zones of ELIP, but it has a sudden decrease below −75 mGal at the beginning of the outer zone and then increases again to ~−20 mGal.

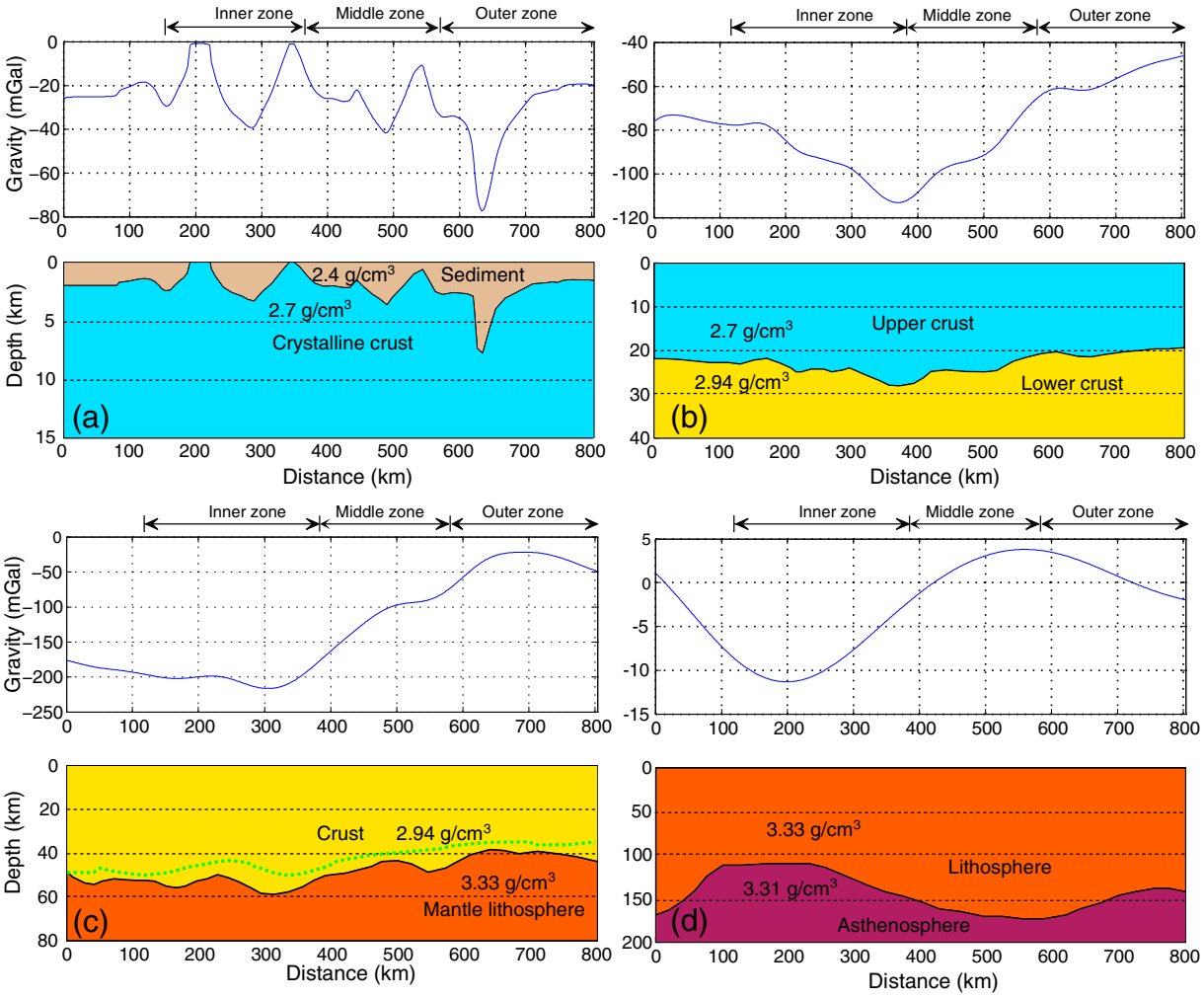

Fig. 4. (a) Gravitational effect of the sediment cover (upper panel) and sediment thickness across the Lijiang–Qingzhen profile (lower panel) (Xu et al., 2014b). (b) Gravitational effect of the undulated upper crust (upper panel) and upper crust thickness along the profile mentioned above (lower panel) (Xu et al., 2015). (c) Moho depth (lower panel) as determined by active-source constraints (green dash line) and also by receiver functions (black continuous line), and gravitational effect of the undulated Moho (upper panel) along the study profile (Chen et al., 2015). (d) Gravitational effect of the undulated LAB (upper panel) and LAB depth along the study profile (lower panel) (Chen et al., in preparation). The density values of the different structures are the ones associated to the reference model (Fig. 3).

3.2. Gravitational effect of the variation in thickness of the upper crust

The crust may be divided into the upper and lower crust. The former has a felsic bulk composition that is similar to granite (Wedepohl, 1995), while the latter has a middle-to-mafic composition (Christensen and Mooney, 1995). Because of this difference in composition, there is a sharp density contrast between the upper and lower crustal layers. Therefore, the undulations of the boundary between these two major layers must be taken into consideration for interpretation of gravity anomaly.

According to the P-wave velocity obtained from the COMWIDE-ELIP experiment (Xu et al., 2015), it is possible to deduce the undulations or the thickness of the upper crust (Fig. 4b, lower plot); the largest depth of the upper crust locates in the boundary between the inner and middle zones. Fig. 4b (upper plot) shows the gravitational effect caused by the undulations of the upper crust and a density contrast of 0.24 g/cm^3 with respect to the reference model (Fig. 3). The gravity anomaly decreases progressively in the inner zone of ELIP to the east and reaches more than −110 mGal at the boundary with the middle zone. From this point to the east, the anomaly rises continuously within the middle and outer zones.

3.3. Gravitational effect of the Moho undulation

Teleseismic receiver functions have proven to be a powerful tool for estimating the crustal thickness (Ammon et al., 1990). By the H-k stacking technique and further migration of receiver functions, Chen et al. (2015) have estimated the Moho depth along the reference profile (Fig. 4c, lower plot). The Moho depth is about 50 km in the inner zone, but reaches 58 km at the boundary with the middle zone. The Moho rises in the middle zone and remains in 40 km in the outer zone of ELIP, so that the difference in the Moho depth could exceed 10 km when going eastward from the inner zone to the outer one. Here, we also present the Moho depth delimited by active-source constraints (green dash line in Fig. 4c) (Xu et al., 2015). In active-source seismology, the energy that propagates down is reflected back when it finds a high-impedance boundary, while the receiver functions, determined from teleseismic data, report on the sampled Moho points. Because the Moho is actually not a thin interface, but a transition zone, the receiver functions detect rather the bottom interface of this transition zone, while the active-source seismic exploration detects its top of interface, which means that active-source method we will get a less Moho depth than receiver functions. Fig. 4c (upper plot) shows the gravitational

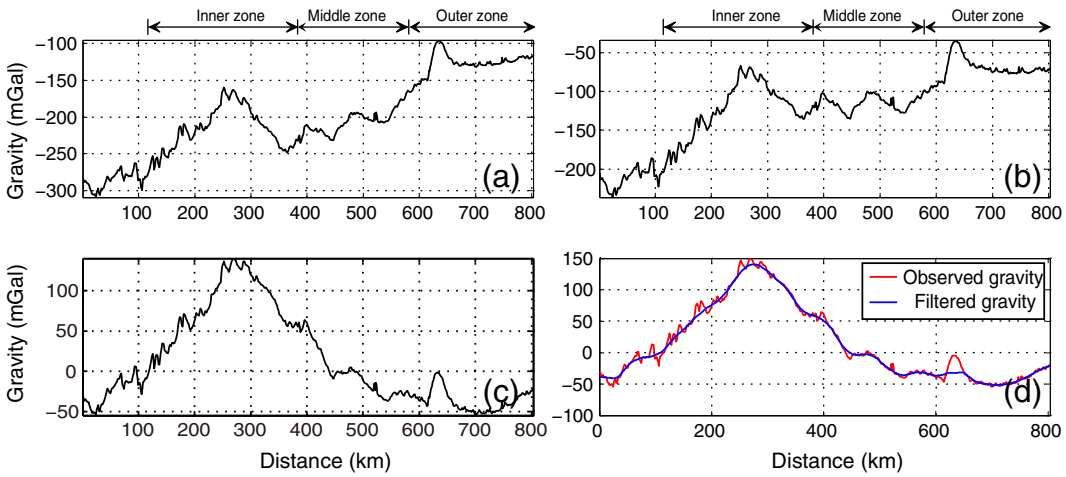

Fig. 5. Stripped residual gravity anomaly after removing successively from the Bouguer gravity the gravitational effects associated to the sediments, crust and upper mantle: (a) Bouguer gravity − $G_{sediment}$; (b) Bouguer gravity − $G_{sediment}$ − G_{crust}; (c) Bouguer gravity − $G_{sediment}$ − G_{crust} − $G_{upper\ mantle}$; (d) Residual gravity (red curly line) and smoothed residual gravity curve (blue line) along the study profile after removing successively the previous gravitational effects. In each case, G refers to the gravitational effect due to the structure (sediment, upper crust, etc.) indicated by the subscript.

effect caused by the Moho undulation, determined by receive functions, and a density contrast of 0.39 g/cm^3 with respect to the reference model (Fig. 3). The negative gravity anomaly reaches −200 mGal in the inner zone of ELIP, in correspondence with the deeper Moho, while it increases in the middle zone and is larger than −50 mGal in the outer zone.

3.4. Gravitational effect of the undulated LAB

Although significantly less, the variations in the thickness of the sub-crustal lithosphere also affect the gravity anomaly measurements. The lithosphere is defined as the cold and rigid outer shell of the Earth through which heat is transmitted by conduction. With the advantage of separating the primary conversions from the multiples by the S-wave arrival times, the S-wave receiver functions are a suitable tool to determine LAB (Kind et al., 2012). Following this method, Chen et al. (in preparation) have obtained the undulations of LAB beneath the passive-source seismic array (Fig. 1). The LAB in ELIP that depicts the mantle lithosphere thickness is shown in Fig. 4d (lower plot). The inner zone has the thinnest lithospheric thickness with a value around 110 km whereas the middle and outer zones have a lithospheric thickness of about 160 km. Fig. 4d (upper plot) shows the gravitational effect of the undulations of LAB calculated with a density contrast of 0.02 g/cm^3 with respect to the reference model (Fig. 3). Given the involved depths around an average value of 150 km, the resultant gravity anomaly is small everywhere. In the inner zone, the gravity anomaly reaches its lowest value of about −10 mGal, while the gravity anomaly is nearly zero in the middle and outer zones.

Table 1
Uncertainties related to the layer thickness, density and induced gravity anomaly. See the text for more details.

Source	Uncertainty in thickness (km)	Uncertainty in density difference (g/cm^3)	Uncertainty in gravity anomaly (mGal)
Observed gravity			1
Sediment	0.5	0.10	~10
Upper crust	2	0.10	~40
Undulation of the Moho	2	0.06	~30
Mantle lithosphere	10	0.02	~10

4. Residual gravity and uncertainties

The step-by-step elimination of the gravitational effects associated with the sediments, the upper crust, the Moho and the lithospheric mantle, allows us to obtain the residual gravity along the study profile as illustrated in Fig. 5. Fig. 5a, b and c present the stripped residual gravity anomaly after removing successively from the Bouguer gravity the gravitational effects associated with the sediments, crust and upper mantle. Fig. 5d presents the final residual gravity. A remarkable positive gravity anomaly extends over the inner and middle zones of the igneous province. The anomaly reaches its largest value of almost 150 mGal in the inner zone, and it decreases gradually in the middle zone and becomes a negative anomaly in the outer zone of ELIP. In order to remove the bias caused mainly by data imprecision and the measurement errors, we used a low-pass filter with the purpose of obtaining the filtered residual gravity (blue line in Fig. 5d), which is the curve that we will consider hereafter.

Regardless of this smoothing, it is important to estimate the errors involved in the calculation of the residual gravity. Deng et al. (2014a) addressed an analysis of this type and reached some important conclusions. The overall error derives from uncertainties in: (1) the gravity measurement and (2) the thickness and density estimated for (a) the sediment; (b) the upper crust; (c) the lower crust; and (d) the mantle lithosphere. Of all these factors, the error associated with the gravity anomaly measurement is the smallest one, given that the observation accuracy with a Burris gravimeter is better than 1 mGal. However, the other factors may give rise to larger errors with a magnitude of 10 mGal or more.

In our gravity modeling, we consider that the density in the sediment, upper crust, lower crust and sub-crustal lithosphere is a constant, which is a simplification of the real conditions considering the data supplied by the boreholes described in Deng et al. (2014a). The standard deviation of the crustal density is based on the uncertainty in the velocity–density formulas given by Christensen and Mooney (1995). For each major crustal layer, this amount is about ±0.05 g/cm^3 (Mooney and Kaban, 2010). We expect that this uncertainty is reduced when we average the densities of several layers, as usually in seismic models of the crust (Mooney and Kaban, 2010). Here, we calculated the gravity anomaly according to the density difference or contrast. The density difference between sediments and the upper crust is 0.24 g/cm^3, but the uncertainty in the average density of the sediments is 0.05 g/cm^3, the same as the uncertainty in the density of the upper crust, so that the uncertainty affecting the density difference around this interface is

Table 2
Numerical results for estimating the source depth and shape.

Window length (s)	z at $q = 0.1$	z at $q = 0.2$	z at $q = 0.3$	z at $q = 0.4$	z at $q = 0.5$	z at $q = 0.6$	z at $q = 0.7$	z at $q = 0.8$	z at $q = 0.9$	z at $q = 1.0$	z at $q = 1.1$	z at $q = 1.2$	z at $q = 1.3$	z at $q = 1.4$	z at $q = 1.5$
40	53.25	55.53	57.73	59.86	61.93	63.94	65.90	67.81	69.68	71.50	73.28	75.03	76.74	78.41	80.06
45	44.69	47.00	49.23	51.38	53.45	55.47	57.43	59.33	61.18	62.99	64.75	66.48	68.17	69.82	71.44
50	36.31	38.68	40.96	43.14	45.25	47.28	49.25	51.16	53.01	54.81	56.56	58.27	59.94	61.57	63.16
55	29.62	32.10	34.47	36.74	38.92	41.02	43.05	45.00	46.89	48.72	50.50	52.23	53.92	55.56	57.16
60	26.28	29.01	31.62	34.13	36.53	38.84	41.06	43.20	45.26	47.26	49.20	51.07	52.89	54.67	56.39
65	27.57	30.68	33.65	36.49	39.21	41.81	44.31	46.72	49.04	51.28	53.46	55.56	57.61	59.60	61.54
70	30.03	33.27	36.36	39.31	42.13	44.84	47.45	49.96	52.39	54.73	57.01	59.22	61.37	63.46	65.51
75	30.42	33.61	36.66	39.59	42.41	45.11	47.72	50.23	52.66	55.02	57.31	59.53	61.70	63.81	65.86
80	28.70	31.68	34.56	37.32	40.00	42.58	45.07	47.49	49.84	52.12	54.34	56.50	58.60	60.66	62.67
85	25.91	28.60	31.18	33.66	36.07	38.39	40.65	42.84	44.97	47.05	49.08	51.07	53.01	54.91	56.77
90	24.41	26.88	29.23	31.46	33.59	35.62	37.57	39.45	41.27	43.03	44.73	46.39	48.01	49.59	51.13
95	23.72	26.01	28.15	30.15	32.03	33.81	35.50	37.11	38.65	40.14	41.57	42.96	44.31	45.62	46.90
100	26.19	28.46	30.52	32.40	34.15	35.77	37.30	38.75	40.14	41.48	42.77	44.03	45.27	46.47	47.66
Average value (km)	31.32	33.96	36.49	38.90	41.20	43.42	45.56	47.62	49.61	51.55	53.43	55.26	57.04	58.78	60.48
Standard deviation	8.65	8.54	8.46	8.42	8.41	8.43	8.48	8.54	8.62	8.72	8.83	8.95	9.08	9.21	9.35

$q = 0.5$ indicates a vertical cylinder for the source; $q = 1.0$ indicates a horizontal cylinder; $q = 1.5$ indicates a sphere.

0.1 g/cm^3. A similar argument is valid for the uncertainty in the average density of the upper and lower crust, which is 0.05 g/cm^3 for the two layers, so the uncertainty in the density difference related to the interface separating both layers is 0.1 g/cm^3. The uncertainty in the average density of the lower crust is 0.05 g/cm^3; but it is hard to determine the average density of the mantle lithosphere. Burov (2010, 2011) considered the density of mantle lithosphere equal to 3.33 g/cm^3, and that of the asthenosphere at 3.31 g/cm^3. We presume the uncertainty in the average density of mantle lithosphere and the asthenosphere is 0.01 g/cm^3, respectively. So the uncertainty in the density difference about the Moho interface is 0.06 g/cm^3, and about LAB is 0.02 g/cm^3. Consequently, the uncertainties in density difference between sediments and upper crust, upper crust and lower crust, crust and mantle lithosphere, lithosphere and asthenosphere are estimated to be 0.1, 0.1, 0.06 and 0.02 g/cm^3, respectively.

In our study, the sediment thickness can be estimated with an error of around 0.5 km using the ray tracing method (Xu et al., 2014b), and hence the error calculated for the gravity anomaly reaches about 10 mGal considering the uncertainty in density mentioned above. Analogously, the upper crust explored by deep seismic sounding yields an uncertainty in thickness less than 2 km (Xu et al., 2015), which corresponds to an error in gravity anomaly of not more than 40 mGal considering the density uncertainty. As the dominant frequency of the Moho converted Ps wave is 1 Hz in the case of the receiver functions calculation, and the average S-wave velocity is close to 3.7 km/s, the wave length comes to be 3.7 km, which corresponds to a resolution of less than 2 km. In such case the uncertainty in the gravity anomaly is less than 30 mGal. Lastly, the uncertainty in the estimation of the lithosphere thickness is generally accepted that is about 10 km, which corresponds to an error in gravity less than 10 mGal. All these uncertainties are summarized in Table 1.

By combining all error sources, the cumulated error inherent to the gravity anomaly varies around 90 mGal along the reference profile. However, it should be noted that all these uncertainties are not correlated and therefore the total uncertainty would be less than the total sum of all of them (Mooney and Kaban, 2010). In summary, the residual gravity anomaly ranges from −50 to +150 mGal (Fig. 5d) yielding a signal-to-noise ratio higher than 2, which is clearly better than the ratio found in our previous analysis (Deng et al., 2014a).

5. Crustal underplating

The interpretation of the residual gravity is often subject to ambiguity due to the multiple solutions for the structure model (Zeng, 2005). Fortunately, our passive seismic investigation has revealed the crustal nature and geometry in the inner zone of ELIP (Chen et al., 2015). Several distinct crustal properties, including high Vp/Vs ratio, low heat flow, a thick crust and the intra-crustal geometry, strongly support a 15- to 20-km-thick mafic layer extending laterally about 150–180 km over the base of the crust in the inner zone (Chen et al., 2015). Second, from active seismology, Xu et al. (2015) have found high P-wave velocity in the lower crust and a P3 interface that is also located at ~35 km depth in the inner zone. Third, the depth of that buried mass is consistent with the depth by using a least-squares variance analysis method (Abdelrahman et al., 2001, 2006), which estimated that the cause of

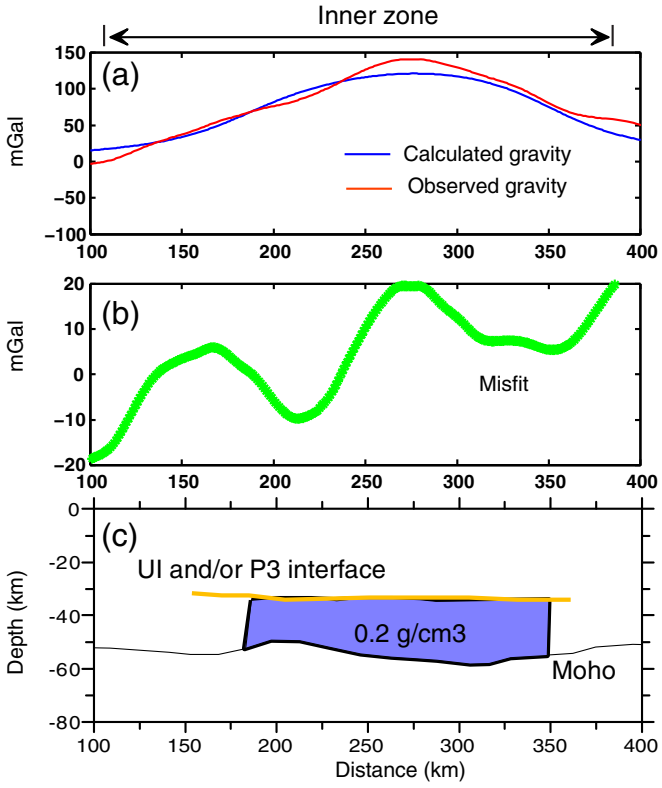

Fig. 6. (a) Adjustment of observed and calculated gravity anomalies in the inner zone of ELIP. (b) Misfit between observed and calculated gravity. (c) 2D average density anomaly model due to crustal underplating. UI means underplating interfaces reported by Chen et al. (2015), while P3 makes reference to the interface found by Xu et al. (2015), in both cases at 35 km depth approximately.

the residual gravity could be a vertical cylinder-shaped body at a depth of 38.9–41.2 km (average values with less variance), in the light of the numerical results concerning the depth of the gravity anomaly source (Table 2).

This mafic layer is interpreted as a result of magmatic underplating related to the Permian mantle plume, and it offers a good starting point to try to explain the gravity anomaly determined by progressive stripping. Owing to the mafic layer formed as a result of this process, such a layer could be the main cause of the residual gravity, although other factors also could contribute to the observed anomaly, which is certainly hard to detect.

By applying the trial-and-error method to the residual gravity, we find the density contrast of 0.2 g/cm^3 for the 15- to 20-km-thick mafic layer overlying the base of the crust (Fig. 6c), which fits reasonably well to the residual gravity in the inner zone of ELIP (Fig. 6a). Other bodies buried in the upper crust and/or in the lithospheric mantle could explain the resultant misfit between observed gravity and calculated gravity (Fig. 6b). But essentially the encountered high density is consistent with the previous geochemical results (Xu et al., 2004; Xu and He, 2007) and accredited geophysical results (Liu et al., 2001; Xu et al., 2014b; Chen et al., 2015), thus providing clear evidence for crustal underplating associated to the past volcanism in Emeishan. This process could be the cause of the non-tectonic uplift of 1–1.5 km in the inner zone of ELIP, such as has been suggested by Chen et al. (2015).

The density contrast of 0.2 g/cm^3 taken as sign of an underplating process admits the comparison with other cases worldwide, namely: 0.2 g/cm^3 in the Early Permian igneous province in Denmark (Thybo and Schönharting, 1991); 0.1 g/cm^3 in the western continental margin of the British Isles (Watts and Fairhead, 1997); 0.15 g/cm^3 in the Mahanadi delta of Eastern India (Behera et al., 2004); 0.12 g/cm^3 in the Rajamal Traps volcanic igneous province in Eastern India (Singh et al., 2004); 0.2 g/cm^3 in the North Atlantic (Sallarès and Calahorrano, 2007); 0.2 g/cm^3 in the South Atlantic margins (Dragoi-Stavar and Hall, 2009); and 0.2 g/cm^3 in the northern Hikurangi margin, New Zealand (Scherwath et al., 2010). Furthermore, numerical simulation of ultramafic magmatic mass intrusion into continental crust (Gerya and Burg, 2007) is also compatible with a very strong density contrast. Therefore, our results seem to further support the presence of a magmatic layer in the lower crust related to the Permian mantle plume.

6. Conclusions

Based on the results provided by recent active- and passive-source seismic experiments, we modeled the residual gravity and the inner density structure in the Emeishan large igneous province in south China. Regarding the first target, we followed a gravity stripping process consisting of the progressive removal of the gravitational effects due to the sediments, the undulated upper crust, the lower crust and the mantle lithosphere. The resultant residual gravity is positive in the inner and middle zones of ELIP, and its strength (up to + 150 mGal) is larger within the inner zone and then decreases gradually in the middle zone and becomes negative in the outer zone.

According to previous knowledge and our latest geophysical observations, we assumed that the residual gravity anomaly beneath the inner zone has its origin in the lower crust. For the density modeling, we considered a simple density model consisting of a 15- to 20-km-thick layer with density contrast of 0.2 g/cm^3 (density of 3.14 g/cm^3) overlying the base of the crust. This model fits reasonably well with the residual gravity in the inner zone, and reveals magmatic underplating in the lower crust associated to the Permian volcanism in ELIP.

Acknowledgements

We want to bring here the memory of Professor Zhongjie Zhang (Liu et al., 2014), who inspired this work and who until recently was the leader of the research group in the IGGCAS. Useful comments made by Prof. Walter D. Mooney, Prof. Yigang Xu and Dr. Qiang Ma helped to greatly improve the manuscript, in addition to constructive suggestions from anonymous reviewers. Some figures were produced using the Generic Mapping Tools software package (Wessel and Smith, 1998). This study was funded by the National Basic Research Program of China (973 Program, grant 2011CB808904) and the State Key Laboratory of Isotope Geochemistry (SKLIG-RC-14-03).

References

Abdelrahman, E.M., El-Araby, T.M., El-Araby, H.M., Abo-Ezz, E.R., 2001. A new method for shape and depth determinations from gravity data. Geophysics 66, 1774–1780.
Abdelrahman, E.M., Abo-Ezz, E.R., Essa, K.S., El-Araby, T.M., Soliman, K.S., 2006. A least-squares variance analysis method for shape and depth estimation from gravity data. J. Geophys. Eng. 3, 143–153. http://dx.doi.org/10.1088/1742-2132/3/2/005.
Ammon, C.J., Randall, G.E., Zandt, G., 1990. On the nonuniqueness of receiver function inversions. J. Geophys. Res. 95, 15303–15318.
Behera, L., Sain, K., Reddy, P.R., 2004. Evidence of underplating from seismic and gravity studies in the Mahanadi Delta of Eastern India and its tectonic significance. J. Geophys. Res. Solid Earth 109, B12311.
Bielik, M., 1988. A preliminary stripped gravity map of the Pannonian Basin. Phys. Earth Planet. Inter. 51 (1–3), 185–189.
Bielik, M., Michael, R., Michael, L., 2013a. Tutorial: the gravity-stripping process as applied to gravity interpretation in the Eastern Mediterranean. Lead. Edge 32 (4), 410–416.
Bielik, M., Krajňák, M., Makarenko, I., Legostaeva, O., Starostenko, V.I., Bošanský, M., Grinč, M., Hók, J., 2013b. 3D gravity interpretation of the pre-Tertiary basement in the intramontane depressions of the Western Carpathians: a case study from the Turiec Basin. Geol. Carpath. 64 (5), 399–408.
Burov, E., 2010. The equivalent elastic thickness (Te), seismicity and the long-term rheology of continental lithosphere: time to burn-out "crème brûlée"? Insights from large-scale geodynamic modeling. Tectonophysics 484 (1), 4–26.
Burov, E.B., 2011. Rheology and strength of the lithosphere. Mar. Pet. Geol. 28, 1402–1443.
Chen, Y., Xu, Y., Xu, T., Si, S., Liang, X., Tian, X., Deng, Y., Chen, L., Wang, P., Xu, Y., Lan, H., Xiao, F., Li, W., Zhang, X., Yuan, X., Badal, J., Teng, J., 2015. Magmatic underplating and crustal growth in the Emeishan large igneous province, SW China, revealed by a passive seismic experiment. Earth Planet. Sci. Lett. 432, 103–114.
Chen, Y., Yuan, X.H., Tian, X.B., Liang, X.F., Deng, Y.F., Badal, J., Xu, Y.G., Teng, J.W., 2016. Lithospheric architecture and origin of the Emeishan large igneous province (SW China) revealed by the COMPASS-ELIP experiment. Geochem. Geophys. Geosyst. (in preparation).
Cheng, L., Zeng, L., Ren, Z., Wang, Y., Luo, Z., 2014. Timescale of emplacement of the Panzhihua gabbroic layered intrusion recorded in giant plagioclase at Sichuan Province, SW China. Lithos 204, 203–219.
Christensen, N.I., Mooney, W.D., 1995. Seismic velocity structure and composition of the continental crust: a global view. J. Geophys. Res. 100 (B6), 9761–9788.
Coffin, M.F., Eldholm, O., 1994. Large igneous provinces: crustal structure, dimensions, and external consequences. Rev. Geophys. 32, 1–36.
Cox, K.G., 1993. Continental magmatic underplating. Philos. Trans. R. Soc. Lond. 342, 155–166.
Deng, Y.F., Li, S.L., Fan, W.M., Liu, J., 2011. Crustal structure beneath South China revealed by deep seismic soundings and its dynamics implications. Chin. J. Geophys. 54 (10), 2560–2574 (in Chinese with abstract in English).
Deng, Y., Zhang, Z., Mooney, W., Badal, J., Fan, W., Zhong, Q., 2014a. Mantle origin of the Emeishan large igneous province (South China) from the analysis of residual gravity anomalies. Lithos 204, 4–13.
Deng, Y., Zhang, Z., Badal, J., Fan, W., 2014b. 3-D density structure under South China constrained by seismic velocity and gravity data. Tectonophysics 627, 159–170.
Dragoi-Stavar, D., Hall, S., 2009. Gravity modeling of the ocean-continent transition along the South Atlantic margins. J. Geophys. Res. Solid Earth 114, B09401.
Gerya, T.V., Burg, J.-P., 2007. Intrusion of ultramafic magmatic bodies into the continental crust: numerical simulation. Phys. Earth Planet. Inter. 160, 124–142.
Hammer, S., 1963. Deep gravity interpretation by stripping. Geophysics 28 (3), 369–378.
He, B., Xu, Y.G., Chung, S.L., Xiao, L., Wang, Y., 2003. Sedimentary evidence for a rapid crustal doming prior to the eruption of the Emeishan flood basalts. Earth Planet. Sci. Lett. 213, 389–403.
He, B., Xu, Y.G., Wang, Y.M., Luo, Z.Y., 2006. Sedimentation and lithofacies paleogeography in SW China before and after the Emeishan flood volcanism: new insights into surface response to mantle plume activity. J. Geol. 114, 117–132.
Jia, Z., Meng, L.S., 2009. Some improvements on the formula for calculating the gravity anomaly due to a 2D homegeneous polygonal source. Prog. Geophys. 24 (2), 462–467 (in Chinese with abstract in English).
Kind, R., Yuan, X., Kumar, P., 2012. Seismic receiver functions and the lithosphere–asthenosphere boundary. Tectonophysics 536–537, 25–43.
Laske, G., Masters, G., Ma, Z., Pasyanos, M., 2013. Update on CRUST1.0, a 1-degree global model of Earth's crust. EGU General Assembly.
Li, Y., Oldenburg, D.W., 1998. 3-D inversion of gravity data. Geophysics 63, 109–119.
Liu, J., Liu, F., He, J., Chen, H., You, Q., 2001. Study of seismic tomography in Panxi paleorift area of Southwestern China—structural features of crust and mantle and their evolution. Sci. China Ser. D Earth Sci. 44, 277–288.
Liu, E.R., Chen, Y., Yang, D.H., Badal, J., Klemperer, S., 2014. Zhongjie Zhang (1964-2013). Tectonophysics 627, 4–5.

Mooney, W.D., Kaban, M.K., 2010. The North American upper mantle: density, composition, and evolution. J. Geophys. Res. 115 (B12), B12424.
Nagy, D., 1966. The gravitational attraction of a right rectangular prism. Geophysics 31 (2), 362–371.
Sallarès, V., Calahorrano, A., 2007. Geophysical characterization of mantle melting anomalies: a crustal view. Geol. Soc. Am. Spec. Pap. 430, 507–524.
Scherwath, M., Kopp, H., Flueh, E.R., Henrys, S.A., Sutherland, R., Stagpoole, V.M., Barker, D.H.N., Reyners, M.E., Bassett, D.G., Planert, L., Dannowski, A., 2010. Fore-arc deformation and underplating at the Northern Hikurangi margin, New Zealand. J. Geophys. Res. Solid Earth 115, B06408.
Shellnutt, J.G., 2014. The Emeishan large igneous province: a synthesis. Geosci. Front. 5 (3), 369–394.
Shellnutt, J.G., Denyszyn, S.W., Mundil, R., 2012. Precise age determination of mafic and felsic intrusive rocks from the Permian Emeishan large igneous province (SW China). Gondwana Res. 22, 118–126.
Singh, A., Kumar, N., Singh, B., 2004. Magmatic underplating beneath the Rajmahal Traps: gravity signature and derived 3-D configuration. J. Earth Syst. Sci. 113, 759–769.
Thybo, H., Artemieva, I.M., 2013. Moho and magmatic underplating in continental lithosphere. Tectonophysics 609, 605–619.
Thybo, H., Schönharting, G., 1991. Geophysical evidence for Early Permian igneous activity in a transtensional environment, Denmark. Tectonophysics 189, 193–208.
Wang, P., Zhang, Z.J., Zhang, X., Han, Y.Y., Wang, M.L., Hou, J., Xu, T., 2014a. Crustal density structure of the Central Longmenshan and adjacent area and its geodynamic implications. Acta Petrol. Sin. 30 (4), 1179–1187 (in Chinese with abstract in English).
Wang, P., Zhang, Z.J., Zhang, X., Han, Y.Y., Wang, M.L., Liang, X.F., Teng, J.W., 2014b. Polygonal grid modeling of 2D complex geological model and calculation of gravity anomaly on Matlab platform. J. Guilin Univ. Technol. 34 (2), 254–259 (in Chinese with abstract in English).
Watts, A.B., Fairhead, J.D., 1997. Gravity anomalies and magmatism along the western continental margin of the British Isles. J. Geol. Soc. 154, 523–529.
Wedepohl, K.H., 1995. The composition of the continental crust. Geochim. Cosmochim. Acta 59 (7), 1217–1232.
Wessel, P., Smith, W.H.F., 1998. New, improved version of the generic mapping tools released. Trans. Am. Geophys. Union 79, 579.
White, R.S., McKenzie, D.P., 1989. Magmatism at rift zones: the generation of volcanic continental margins and flood basalts. J. Geophys. Res. 94, 7685–7729.
Wignall, P., Sun, Y., Bond, D.P.G., Izon, G., Newton, R.J., Védrine, S., Widdowson, M., Ali, J.R., Lai, X., Jiang, H., 2009. Volcanism, mass extinction, and carbon isotope fluctuations in the middle Permian of China. Science 324, 1179–1182.
Wu, J., Zhang, Z., 2012. Spatial distribution of seismic layer, crustal thickness, and Vp/Vs ratio in the Permian Emeishan mantle plume region. Gondwana Res. 22 (1), 127–139.
Xu, Y.G., He, B., 2007. Thick and high velocity crust in Emeishan large igneous province, SW China: evidence for crustal growth by magmatic underplating/intraplating. The origins of melting anomalies: plates, plumes, and planetary processes. In: Foulger, G., Jurdy, D. (Eds.), Geological Society of America, Special Publication 430, pp. 841–858.
Xu, Y.G., Chung, S.L., Jahn, B.M., Wu, G.Y., 2001. Petrologic and geochemical constraints on the petrogenesis of Permian–Triassic Emeishan flood basalts in Southwestern China. Lithos 58, 145–168.
Xu, Y.G., He, B., Chung, S., Menzies, M.A., Frey, F.A., 2004. Geologic, geochemical, and geophysical consequences of plume involvement in the Emeishan flood-basalt province. Geology 32 (10), 917–920.
Xu, Y.G., He, B., Huan, X.L., Luo, Z.Y., Chung, S.L., Xiao, L., Zhu, D., Shao, H., Fan, W.M., Xu, J.F., Wang, Y.J., 2007. Identification of mantle plumes in the Emeishan large igneous province. Episodes 30, 32–42.
Xu, Y.G., Wang, C.Y., Shen, S., 2014a. Permian large igneous provinces: characteristics, mineralization and paleo-environment effects. Lithos 204, 1–3.
Xu, T., Zhang, M.H., Tian, X.B., Zheng, Y., Bai, Z.M., Wu, C.L., Zhang, Z.J., Teng, J.W., 2014b. Upper crustal velocity of Lijiang–Qingzhen profile and its relationship with the seismogenic environment of the MS 6.5 Ludian earthquake. Chin. J. Geophys. 57 (9), 3069–3079.
Xu, T., Zhang, Z.J., Liu, B.F., Chen, Y., Zhang, M.H., Tian, X.B., Xu, Y.G., Teng, J.W., 2015. Velocity structure of the crust along Emeishan large igneous province and active traces of ancient mantle plume: constraints from active source seismic experiment along the Lijiang to Qingzhen profile in China. Sci. China Ser. D Earth Sci. 58 (7), 1133–1147.
Yuan, D.X., Shen, S.Z., Henderson, C.M., Chen, J., Zhang, H., Feng, H.Z., 2014. Revised conodont-based integrated high-resolution timescale for the Changhsingian stage and end-Permian extinction interval at the Meishan sections, South China. Lithos 204, 220–245.
Zeng, H.L., 2005. Gravity Field and Gravity Exploration. Geological Publishing House, Beijing, pp. 79–100.
Zhang, Z., Klemperer, S., 2010. Crustal structure of the Tethyan Himalaya, Southern Tibet: new constraints from old wide-angle seismic data. Geophys. J. Int. 181, 1247–1260.
Zhang, Z., Zhao, B., Zhang, X., Liu, C., 2006. Crustal structure beneath the wide-angle seismic profile between Simao and Zhongdian in Yunnan. Chin. J. Geophys. 49 (5), 1377–1384 (in Chinese with abstract in English).
Zhang, R., He, Z.T., Guo, S.S., Li, H., Hao, X.S., 2011. Characteristics test of Burris gravimeter. J. Geod. Geodyn. 31 (6), 155–158.
Zhang, Z., Xu, T., Zhao, B., Badal, J., 2013. Systematic variations in seismic velocity and reflection in the crust of Cathaysia: new constraints on intraplate orogeny in the South China continent. Gondwana Res. 24, 902–917.
Zhong, Y.T., He, B., Mundil, R., Xu, Y.G., 2014. CA-TIMS zircon U–Pb dating of felsic ignimbrite from the Binchuan section: implications for the termination age of Emeishan large igneous province. Lithos 204, 14–19.